

Self-optimization, community stability, and fluctuations in a class of individual-based models of biological coevolution

Per Arne Rikvold

*School of Computational Science, Center for Materials Research and Technology,
National High Magnetic Field Laboratory, and Department of Physics,
Florida State University, Tallahassee, Florida 32306-4120, USA
and Department of Fundamental Sciences, Faculty of Integrated Human Studies,
Kyoto University, Kyoto 606, Japan*

Abstract

We study the dynamical properties of a class of simple, individual-based models of biological coevolution. These are multispecies, stochastic population-dynamics models in which the reproduction probability for individuals of a particular species depends nonlinearly on the population densities of all the species present in the community. New species are introduced through a small probability of mutation during reproduction. For a subclass of simplified models we are able to perform exact linear stability analysis, and we compare the analytic results with large-scale kinetic Monte Carlo simulations. Based on this analysis, we present a phase diagram for the total population size as a function of an average interspecies interaction strength. Over time, the models are found to *self-optimize* through mutation and selection to maximize a community fitness function, subject only to constraints internal to the particular model. If the off-diagonal elements of the matrix of interspecies interactions are distributed independently on an interval that includes positive values, the model evolves toward *mutualistic* communities, in which the population is self-sustaining. In contrast, for predator/prey models the interaction matrix is antisymmetric, and the community is constrained to a region of the phase diagram where a nonzero population size can only be sustained by an external resource. Time series of the diversity and total population size for the different models show approximate $1/f$ noise and power-law distributions for the lifetimes of communities and species. For the mutualistic model, these two lifetime distributions have the same exponent, while their exponents are different for the predator/prey model. The difference is probably due to greater resilience toward mass extinctions exhibited by the food-web like communities produced by the predator/prey model.

Key words: Evolution, Self-optimization, Community stability, Mutualistic interactions, Predator-prey interactions, Power laws

1 Introduction

Traditionally, problems in ecology and evolution have been addressed at very different levels of resolution. Typically, ecological problems are addressed on a timescale of generations and often at the level of individual organisms, while issues in evolution are considered on much longer, often geological, timescales and usually at the level of species or even higher-level taxa. However, in recent years it has been recognized that processes at the ecological and evolutionary scales can be strongly linked (Thompson, 1998, 1999; Drossel et al., 2001; Yoshida et al., 2003). Several models have therefore been proposed, which aim to model the resulting complex problem of coevolution in a fitness landscape that changes with the composition of the community, while spanning the disparate scales of both temporal and taxonomic resolution. Early steps in this direction were simulations of allopatric speciation by Crosby (1970) and the coupled NK model with population dynamics introduced by Kauffman and Johnsen (1991) (see also Kauffman, 1993). More recent contributions include the Webworld model (Caldarelli et al., 1998; Drossel et al., 2001, 2004), the Tangled-nature model (Christensen et al., 2002; Hall et al., 2002; di Collobiano et al., 2003), and simplified versions of the latter (Rikvold and Zia, 2003; Zia and Rikvold, 2004; Sevim and Rikvold, 2005), as well as the network models due to Chowdhury et al. (2003) (see also Chowdhury and Stauffer, 2005, and references therein). Recently, large individual-based simulations have also been performed of parapatric and sympatric speciation (Gavrilets and Boake, 1998; Gavrilets et al., 2000) and of adaptive radiation (Gavrilets and Vose, 2005). Many of these models are deliberately quite simple, aiming to elucidate *universal* features that are largely independent of the finer details of the ecological interactions and the evolutionary mechanisms. Such universal features may include lifetime distributions for species and communities, as well as other aspects of extinction statistics, statistical properties of fluctuations in diversity and population sizes, and the structure and dynamics of food webs that develop and change on both the ecological and evolutionary time scales. By changing specific features of the various simplified models, one hopes to learn which aspects of the models are linked to the observed properties of the resulting communities and their development with time.

In this paper we investigate a class of stochastic, individual-based coevolution models, which combine features from some of those mentioned above. We first define the class in general, and then proceed to study two specific members, both analytically by linear stability theory, and numerically by large-scale kinetic Monte Carlo simulations. One of these models (which we call

Email address: rikvold@scs.fsu.edu (Per Arne Rikvold).

URL: www.physics.fsu.edu/users/rikvold/info/rikvold.html (Per Arne Rikvold).

Model A) allows direct mutualistic interspecies interactions, and many of its properties have been discussed in previous work by the author and coworkers (Rikvold and Zia, 2003; Zia and Rikvold, 2004; Sevim and Rikvold, 2005). It is a simplified version of the Tangled-nature model (Christensen et al., 2002; Hall et al., 2002; di Collobiano et al., 2003). The second model (which we call Model B) is a predator/prey model. Both models contain simplifying features that enable us to obtain the fixed-point mean population sizes and stability properties for any given community of species exactly in the limit of vanishing mutation rate, using linear stability theory. These results enable us to define a *community fitness function*, cubic in the mean total population size, that is maximized at the fixed point for a given community of species.

The analytical results are followed by numerical simulations of the dynamics of both models for nonzero mutation rates. We focus on very long simulations in a regime where both diversity and population size are statistically stationary, albeit with very large, strongly correlated fluctuations and an intermittently vigorous turnover of species. We are thus able to study the *intrinsic* dynamics of extinction and origination of species and communities in the absence of external perturbations. Understanding of these intrinsic fluctuations in the stationary state should enable one to estimate the population's susceptibility to external influences, in a way inspired by the well-known fluctuation-dissipation relations of statistical mechanics (see, e.g., Pathria, 1996, Chs. 11 and 14).

Three main conclusions emerge from this combined analytical and numerical investigation.

- Mutations enable the models to evolve communities that maximize the community fitness function, subject only to constraints that are internal to the specific model. Although there is vigorous turnover of species and communities, all communities that persist for a significant time remain close to this maximum.
- The simulated systems exhibit power-law distributions in the lifetimes of individual species, as well as of communities, and the fluctuations in diversity and population size are characterized by approximate $1/f$ noise.
- The two models show distinct differences in the community turnover, which are reflected in differences between the power-law exponent of the community-lifetime distribution. In Model A, extinctions of species tend to be highly synchronized, such that a whole community collapses in a mass extinction on a relatively short time scale. In Model B, on the other hand, extinctions are more often limited to a subset of the resident species. This difference can be explained by differences between the structures of the interaction networks characterizing long-lived communities in the two models. For Model B, this network amounts to a simple food web.

The rest of this paper is organized as follows. The general class of models is introduced in Sec. 2. In Sec. 3 we introduce the simplifications that make the models amenable to a full analytical linear-stability analysis. Such analysis is performed, and the results are compared with results from large-scale kinetic Monte Carlo simulations. The simulations are described in further detail in Sec. 4, where lifetime distributions and power-spectral densities also are reported. A concluding summary is presented in Sec. 5. Some technical details of the derivation of the community fitness function are given in Appendix A, and a discussion of the consequences of changes in several of the model parameters is found in Appendix B.

2 General Model

In the models studied here, selection is provided by the reproduction rates in an individual-based, simplified population-dynamics model with nonoverlapping generations, similar to a multispecies, stochastic Lotka-Volterra model (Murray, 1989). This interacting birth/death process is augmented to enable evolution of new species by a mutation mechanism. The mutations act on a haploid, binary “genome” of length L , as introduced by Eigen in his model for molecular evolution (Eigen, 1971; Eigen et al., 1988). This bit string defines the species, which are identified by the integer label $I \in [0, 2^L - 1]$. Typically, only a few of these 2^L potential species are resident in the community at any one time.

Individual organisms of species I reproduce asexually at the end of each generation, each giving rise to F offspring individuals with probability P_I before dying. With probability $(1 - P_I)$, they die without offspring. No individual thus survives beyond one generation. (For simplicity, the fecundity F is assumed fixed, independent of both species and individual.)

During reproduction, each gene in an offspring individual’s genome may undergo mutation ($0 \rightarrow 1$ or $1 \rightarrow 0$) with a small probability, μ/L . The mutation thus corresponds to diffusional moves from corner to corner along the edges of an L -dimensional hypercube (Gavrilets, 1999, 2004). A mutated individual is assumed to belong to a different species than its parent, with different properties. Genotype and phenotype are thus in one-to-one correspondence in these models. This is clearly a highly idealized picture, and it is introduced to maximize the pool of different species available within the computational resources. The approximation is justified by a large-scale computational study of a version of Model A, in which species that differ by as many as $L/2$ bits have correlated properties (Sevim and Rikvold, 2005). Quite remarkably, this study reveals that the more realistic, correlated model has long-time dynamical properties very similar to the uncorrelated Model A studied here.

The reproduction probability $P_I(t)$ for an individual of species I in generation t depends on the individual’s ability to utilize the amount of external resources available, R , and on its interactions with the population sizes $n_J(t)$ of all the species present in the community at that time. (We emphasize that the population size $n_J(t)$ is the number of individuals of species J in generation t . It is thus restricted to being an integer ≥ 0 .) The dependence of P_I on the set of n_J is determined by an *interaction matrix* \mathbf{M} (Solé et al., 1996) with elements $M_{IJ} \in [-1, 1]$ in a way defined specifically in the next paragraph. We emphasize that \mathbf{M} is chosen randomly at the beginning of each simulation run and is subsequently kept *constant* throughout the run. If M_{IJ} is positive and M_{JI} is negative, then I is a predator and J its prey, and *vice versa*. If both matrix elements are positive, the species interact directly in a mutualistic way, while both elements negative implies direct competition.

Specifically, the reproduction probability for species I , $P_I(t)$, depends on R and the set $\{n_J(t)\}$ through the nonlinear form,

$$P_I(t) = \frac{1}{1 + \exp[-\Delta_I(R, \{n_J(t)\})]} , \quad (1)$$

where

$$\Delta_I(R, \{n_J(t)\}) = -b_I + \eta_I R f_1 + \sum_J M_{IJ} f_2 g_2 n_J(t) - N_{\text{tot}}(t)/N_0 . \quad (2)$$

Here b_I can be seen as the “cost” of reproduction (always positive), and η_I (positive for primary producers or autotrophs, and zero for consumers or heterotrophs) is the ability of individuals of species I to utilize the external resource R . The latter is an abiotic resource that is renewed at the same level each generation. It does *not* have independent dynamics. The factors f_1 and f_2 are in general functions of the population sizes that represent competition for resources (f_1) or prey (f_2), and g_2 is a function that expresses the ability of a predator to engage in adaptive foraging (Drossel et al., 2004). The total population size is $N_{\text{tot}}(t) = \sum_J n_J(t)$. [In contrast, the total number of *species* present in generation t (the species richness) will be defined as $\mathcal{N}(t)$.] The constant N_0 is an environmental carrying capacity (a.k.a. a Verhulst factor) (Murray, 1989; Verhulst, 1838), which prevents the population size from diverging to infinity. For large positive Δ_I , the individual almost certainly reproduces, giving rise to F offspring. In the opposite limit of large negative Δ_I , it almost certainly dies without offspring. The reproduction probability P_I , together with the specific form of its argument, $\Delta_I(R, \{n_J\})$, play the role of a functional response for this class of models (Drossel et al., 2001; Krebs, 2001, Chs. 13–14). The model parameters are chosen to represent the realistic situation that the number of species that exist in the community at any time

is much smaller than the number of potential species (i.e., that $\mathcal{N}(t) \ll 2^L$), and also that $\mathcal{N}(t) \ll N_{\text{tot}}(t)$.

An analytic approximation describing the development in time of the mean values of the population sizes (averaged over independent realizations), $\langle n_I(t) \rangle$, can be written as a set of coupled difference equations,

$$\begin{aligned} \langle n_I(t+1) \rangle = & \langle n_I(t) \rangle F P_I(R, \{\langle n_J(t) \rangle\}) [1 - \mu] \\ & + (\mu/L) F \sum_{K(I)} \langle n_{K(I)}(t) \rangle P_{K(I)}(R, \{\langle n_J(t) \rangle\}) + O(\mu^2), \end{aligned} \quad (3)$$

where $K(I)$ is the set of species that can be generated from species I by a single mutation (“nearest neighbors” of I in genotype space).

3 Simplified Models

A very simple choice of parameters in Eq. (2) is $f_1 = f_2 = 1/N_{\text{tot}}(t)$ and $g_2 = 1$. This represents frequency-dependent interactions that describe universal competition and absence of adaptive foraging, and so is not very realistic. However, it has the advantage that it turns Eq. (3) in the absence of mutations (i.e., with $\mu = 0$) into a set of linear equations for the average population sizes in a fixed-point community. This set can be solved analytically to give the average population size of each species, as well as the average total population size and the stability properties of the community. In this paper we consider specifically two such simplified models, which can serve as benchmarks for future studies of models involving more realistic choices of f_1 , f_2 , and g_2 .

3.1 Model A

The first of these models, Model A, is the one introduced and studied by Rikvold and Zia (2003) (see also Zia and Rikvold, 2004; Sevim and Rikvold, 2005). In this model, the M_{IJ} for $I \neq J$ are stochastically independent and uniformly distributed on $[-1, +1]$, while the intra-species interactions $M_{II} = 0$. The external resource R and the reproduction costs b_I are all equal to zero, and the total population size $N_{\text{tot}}(t)$ is limited only by the carrying capacity N_0 .

3.2 Model B

The second model, Model B, is a predator-prey model. This is implemented by making the off-diagonal part of \mathbf{M} antisymmetric. In order to keep the connectance of the resulting communities consistent with food webs observed in nature (Dunne et al., 2002; Garlaschelli, 2004, and references therein), the (M_{IJ}, M_{JI}) pairs are chosen nonzero with probability $c = 0.1$. The nonzero elements in the upper triangle of \mathbf{M} are chosen independently and uniformly on $[-1, +1]$. This model does not include a population-limiting carrying capacity [i.e., formally, $N_0 = \infty$ in Eq. (2)], and the community is supported by a constant external resource, R . Only a proportion p of the 2^L potential species are producers that can directly utilize the resource (for the numerical data reported here, we use $p = 0.05$). Thus, with probability $(1 - p)$ the resource coupling $\eta_I = 0$, representing consumers, while with probability p the η_I are independently and uniformly distributed on $(0, +1]$, representing producers of varying efficiency. In addition to the constraints on \mathbf{M} mentioned above, we require that producers ($\eta_I > 0$) always are the prey of consumers ($\eta_I = 0$). Consumers at higher trophic levels are allowed, and they are indeed observed in the resulting communities (see further discussion in Sec. 4). The population sizes are limited by independent reproduction costs b_I that are uniformly distributed on $(0, +1]$, and by negative intra-species interactions M_{II} independently and uniformly distributed on $[-1, 0)$.

Some preliminary numerical results for Model B were presented by Rikvold (2005). An extensive numerical study, focusing solely on this model, will be published elsewhere (Rikvold, in preparation).

3.3 Fixed-point communities

To obtain the stationary solution of Eq. (3) with $\mu = 0$ for a community of \mathcal{N} species, we must require $P_I = 1/F$ for all \mathcal{N} species. Equations (1) and (2) then give rise to the \mathcal{N} linear relations

$$-\tilde{b}_I + \eta_I \frac{R}{N_{\text{tot}}^*} + \sum_J M_{IJ} \frac{n_J^*}{N_{\text{tot}}^*} - \frac{N_{\text{tot}}^*}{N_0} = 0, \quad (4)$$

where $\tilde{b}_I = b_I - \ln(F - 1)$. (For simplicity, we have dropped the $\langle \rangle$ notation for the average population sizes, and the asterisk superscripts denote fixed-point solutions.) In a convenient vector notation, $|n^*\rangle$ is the column vector composed of the \mathcal{N} nonzero n_I^* , while $\langle 1|$ is an \mathcal{N} -dimensional row vector composed entirely of ones. Thus, the total population size is given by the

inner product, $N_{\text{tot}}^* = \langle 1|n^* \rangle = \sum_I n_I^*$, and Eq. (4) takes the matrix form

$$-|\tilde{b}\rangle N_{\text{tot}}^* + R|\eta\rangle + \hat{\mathbf{M}}|n^*\rangle - |1\rangle(N_{\text{tot}}^*)^2/N_0 = 0. \quad (5)$$

Here, $|\tilde{b}\rangle$ is the column vector whose elements are \tilde{b}_I , $|\eta\rangle$ is the column vector whose elements are η_I (in both cases including only those \mathcal{N} species that have nonzero n_I^*), $\hat{\mathbf{M}}$ is the corresponding $\mathcal{N} \times \mathcal{N}$ submatrix of \mathbf{M} , and $|1\rangle$ is an \mathcal{N} -dimensional column vector of ones. The solution for $|n^*\rangle$ is

$$|n^*\rangle = -\hat{\mathbf{M}}^{-1} \left[|\eta\rangle R - |\tilde{b}\rangle N_{\text{tot}}^* - |1\rangle(N_{\text{tot}}^*)^2/N_0 \right], \quad (6)$$

where $\hat{\mathbf{M}}^{-1}$ is the inverse of $\hat{\mathbf{M}}$. (See below for a discussion of the effect of a singular $\hat{\mathbf{M}}$.) To find each n_I^* , we must first obtain $N_{\text{tot}}^* \equiv \langle 1|n^* \rangle$. Multiplying Eq. (6) from the left by $\langle 1|$, we obtain the quadratic equation for N_{tot}^* ,

$$R\mathcal{E} + \Theta N_{\text{tot}}^* - (N_{\text{tot}}^*)^2/N_0 = 0. \quad (7)$$

The coefficients,

$$\Theta = \frac{1 - \langle 1|\hat{\mathbf{M}}^{-1}|\tilde{b}\rangle}{\langle 1|\hat{\mathbf{M}}^{-1}|1\rangle} \quad \text{and} \quad \mathcal{E} = \frac{\langle 1|\hat{\mathbf{M}}^{-1}|\eta\rangle}{\langle 1|\hat{\mathbf{M}}^{-1}|1\rangle}, \quad (8)$$

can be viewed as an effective interaction strength and an effective coupling to the external resource, respectively. Approximate expressions for Θ and \mathcal{E} that are less accurate but more intuitive are obtained in Appendix A. The nonnegative solution of Eq. (7) is

$$N_{\text{tot}}^* = \frac{\Theta N_0}{2} + \sqrt{\left(\frac{\Theta N_0}{2}\right)^2 + R\mathcal{E}N_0}. \quad (9)$$

Figure 1(a) shows N_{tot}^* as a function of Θ for two choices of N_0 and R at fixed \mathcal{E} . Special cases of the solution are

$$N_{\text{tot}}^* = \begin{cases} \Theta N_0 & \text{for } R = 0 \quad \text{and} \quad \Theta \geq 0 \\ 0 & \text{for } R = 0 \quad \text{and} \quad \Theta \leq 0 \\ \sqrt{R\mathcal{E}N_0} & \text{for } \Theta = 0 \quad \text{and} \quad \mathcal{E} \geq 0 \\ -R\mathcal{E}/\Theta & \text{for } N_0 = \infty \quad \text{and/or} \quad \langle 1|\hat{\mathbf{M}}^{-1}|1\rangle = 0 \end{cases}. \quad (10)$$

To find each n_I^* separately, we now only need to insert the solution for N_{tot}^* in Eq. (6).

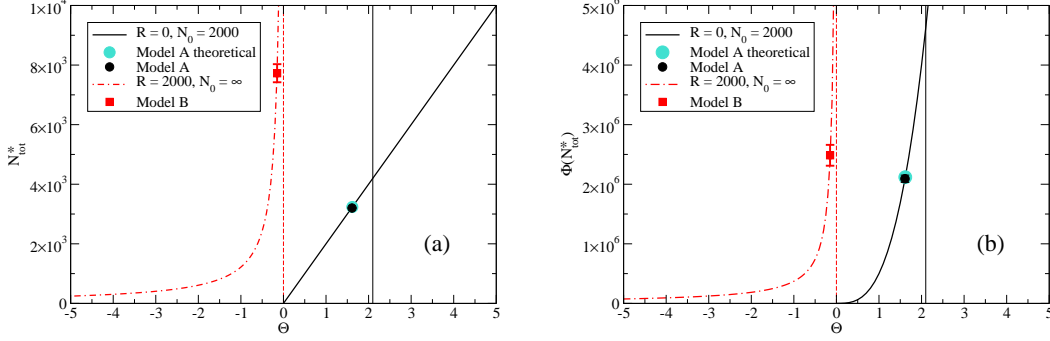


Fig. 1. (Color online.) Results of the mean-field approximation for **(a)** The total fixed-point population size N_{tot}^* and **(b)** the community fitness function $\Phi(N_{\text{tot}}^*)$. Both are shown vs Θ for fixed $\mathcal{E} = 0.61$. The solid vertical lines represent the absolute maximum value for Θ in Model A, while the dotted vertical lines represent the analogous limit for Model B. The points marked “Model A” and “Model B” were obtained from large-scale Monte Carlo simulations as described in the text. The calculation of the point marked “Model A theoretical” is also described in the text.

Only those $|n^*\rangle$ that have all positive elements can represent a *feasible* community (Roberts, 1974). If $\hat{\mathbf{M}} = \mathbf{0}$ or is otherwise singular, the set of equations (5) is inconsistent for $\mathcal{N} > 1$, unless \tilde{b}_I and η_I both are independent of I (this case is equivalent to $\mathcal{N} = 1$). The only possible stationary community then consists of one single species, the one with the largest value of η_I/\tilde{b}_I . This is a trivial example of competitive exclusion (Hardin, 1960; Armstrong and McGehee, 1980; den Boer, 1986).

Equation (7) can be seen as a maximization condition for a “community fitness” function,

$$\Phi(N_{\text{tot}}) = \left(1 - \frac{1}{F}\right) \left(R\mathcal{E}N_{\text{tot}} + \frac{\Theta}{2}N_{\text{tot}}^2 - \frac{1}{3N_0}N_{\text{tot}}^3\right), \quad (11)$$

which is cubic in N_{tot} .¹ The dependence of Φ on N_{tot} is shown in Fig. 2 for Models A and B at two different values of Θ . The maximum value of Φ with respect to N_{tot} , $\Phi(N_{\text{tot}}^*)$, is shown in Fig. 1(b) vs Θ for two different values of N_0 at fixed \mathcal{E} .

From Eq. (10) and Fig. 1(a) it is seen that Model A (finite N_0 and $R = 0$) undergoes a transcritical bifurcation or exchange of stabilities (Crawford, 1991; Strogatz, 1994, Ch. 3) at $\Theta = 0$. For $\Theta \leq 0$, N_{tot} vanishes, while for $\Theta > 0$ it

¹ Here we have obtained Eq. (11) simply by integration of Eq. (7). A conventional mean-field derivation, which also explains the prefactor $(1 - 1/F)$ and provides intuitive approximations for Θ and \mathcal{E} , is given in Appendix A.

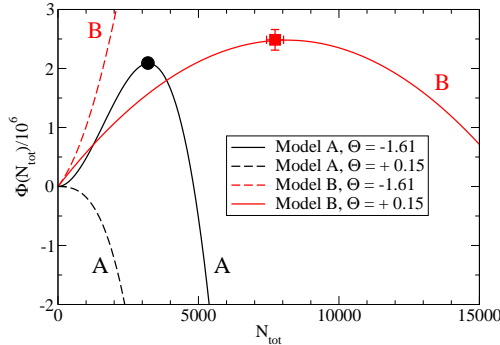


Fig. 2. (Color online.) The community fitness function $\Phi(N_{\text{tot}})$, shown vs N_{tot} for Model A (black) and Model B (gray, red online). For Model A the parameters are: $F = 4$, $R = 0$, and $N_0 = 2000$. For Model B they are: $F = 2$, $R = 2000$, $\mathcal{E} = 0.61$, and $N_0 = \infty$. The values of Θ used are 1.61, corresponding to the average value taken by Model A in the simulations, and -0.15 , corresponding to the average value taken by Model B. $\Phi(N_{\text{tot}})$ has a nontrivial maximum for Model A at positive Θ (solid black curve marked A), and for Model B at negative Θ (solid gray curve marked B (red online)). The circular and square data points are the results of Monte Carlo simulations and correspond to the equally shaped points in Fig. 1. They lie very close to the maximum of $\Phi(N_{\text{tot}})$ for each model. The dashed curves show the physically inaccessible cases of Model A with $\Theta < 0$ (stable, absorbing state at $N_{\text{tot}} = 0$) and Model B with $\Theta > 0$ (monotonically increasing $\Phi(N_{\text{tot}})$).

increases linearly with Θ .² Such behavior as a function of a control parameter is common in many nonequilibrium systems. In addition to population dynamics and the logistic map (to which the present systems with $\mu = 0$ are closely related), these also include lasers and autocatalytic chemical reactions (Haken, 1977; Strogatz, 1994). On the other hand, for Model B ($N_0 = \infty$ and $R > 0$), N_{tot} diverges to infinity as Θ approaches zero from below, and it would be infinite for $\Theta \geq 0$.

The results discussed in the previous paragraph would not be very interesting if Θ were a fixed control parameter, as it would be in the absence of extinctions and mutations. However, mutations enable the community not only to maximize $\Phi(N_{\text{tot}})$ for fixed parameters, *but also to increase it further as new, favorable mutations appear*. Numerically we find that the community progresses toward, and then settles down to fluctuate near, the maximum value of Θ (and thus the maximum value of $\Phi(N_{\text{tot}}^*)$) compatible with the constraints on \mathbf{M} and $|\tilde{b}\rangle$. These constraints depend on the specific model as follows. For Model A, which allows direct mutualistic interactions (i.e., M_{IJ} and M_{JI} both positive), Θ can be positive, thus enabling communities with nonzero population size, even for $R = 0$. For the predator/prey Model B, on the other hand, the antisymmetric structure of \mathbf{M} forces Θ to be nonpositive.

² In the presence of a positive external resource ($R > 0$) the bifurcation for Model A would become *imperfect* (Strogatz, 1994, Ch. 3), yielding positive N_{tot} for all Θ , as is easily seen from Eq. (9).

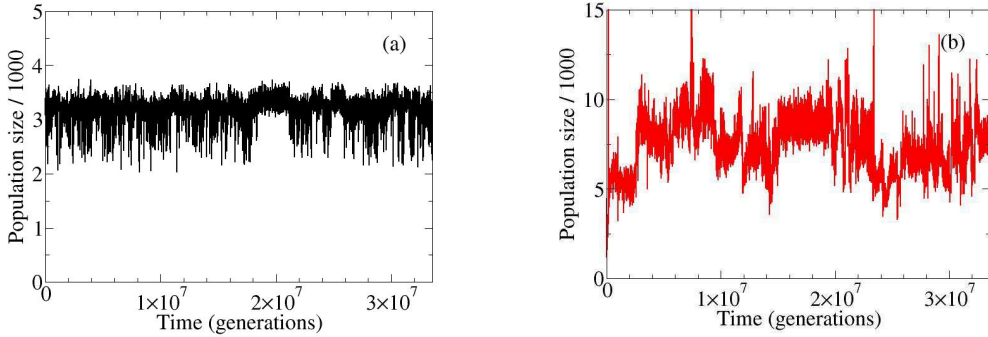


Fig. 3. (Color online.) Typical time series of the total population sizes, $N_{\text{tot}}(t)$, for Monte Carlo runs of $2^{25} = 33\,554\,432$ generations each. To reduce the size of the figure file, the data are sampled only once every 2048 generations. While this slightly reduces the apparent range of the short-time fluctuations, the general shapes of the time series are preserved. **(a)** Model A: $N_0 = 2000$, $R = 0$, $F = 4$, $L = 13$, and $\mu = 10^{-3}$. **(b)** Model B: $N_0 = \infty$, $R = 2000$, $F = 2$, $L = 13$, and $\mu = 10^{-3}$.

In Monte Carlo simulations of Model A (in which the offdiagonal elements of \mathbf{M} are uncorrelated and uniformly distributed on $[-1, +1]$), it was found that the community spent most of its time in a succession of quasi-steady states (QSS), separated by brief bursts of intense evolutionary activity (Rikvold and Zia, 2003). All the QSS studied in detail were found to be mutualistic, with $\overline{M_{IJ}} = 0.78 \pm 0.03$ and $\overline{\Theta} = 1.61 \pm 0.01$. [Here, the overbar represents averages over all the ten QSS listed in Table I of Rikvold and Zia (2003).] The average of N_{tot} , taken over all the 16 realizations of 2^{25} generations that were studied, was $\overline{N_{\text{tot}}} = 3201 \pm 8$. (The average over only the ten QSS agrees with the total average to within the statistical errors, showing that the periods when the system is not in a QSS contribute negligibly to the overall time averages.) In Fig. 1(a), $\overline{N_{\text{tot}}}$ is shown vs $\overline{\Theta}$ as a black dot, while the corresponding value of $\Phi(\overline{N_{\text{tot}}})$ is shown the same way in Fig. 1(b). A typical time series of $N_{\text{tot}}(t)$ for Model A is shown in Fig. 3(a).

We can obtain a theoretical estimate for the point $(\overline{\Theta}, \overline{N_{\text{tot}}})$ in Model A. We assume for simplicity that all the offdiagonal M_{IJ} have the same value, a . Then, using the definition of Θ , and remembering that $F = 4$ for Model A, so that $\tilde{b}_I = -\ln 3$ for all I , one can show that $\Theta = (1 - 1/\mathcal{N})a + \ln 3$, where \mathcal{N} is the total number of species in the community. This yields the absolute maximum value for Θ equal to $(1 + \ln 3) \approx 2.10$ for $\mathcal{N} = \infty$ (shown by vertical full lines in Fig. 1). However, it was shown by Rikvold and Zia (2003) that the most probable number of species in a community is finite and given by

$$\mathcal{N}^\dagger \approx L \ln 2 / \ln(1/q), \quad (12)$$

where q is the probability of finding a pair of interactions, M_{IJ} and M_{JI} , conducive to this community. With the M_{IJ} independently distributed on

$[-1, +1]$, the probability of drawing a pair that are both larger than some given value $m \in [-1, +1]$, is $q = [(1 - m)/2]^2$. In our approximate formula for Θ , we now replace \mathcal{N} by \mathcal{N}^\dagger with this value of q , and a by the average of a variable uniformly distributed over $[m, 1]$, which is $(1 + m)/2$. This yields

$$\Theta \approx \left[1 - \frac{2 \ln \left(\frac{2}{1-m} \right)}{13 \ln 2} \right] \frac{1+m}{2} + \ln 3 \quad (13)$$

for $L = 13$. This is a concave function of m with a single maximum at m_{\max} , which can be found numerically. The result is $m_{\max} \approx 0.512$, which yields $\Theta_{\max} \approx 1.618$, $N_{\text{tot}} \approx 3236$, and $\overline{M}_{IJ} = (1 + m_{\max})/2 \approx 0.756$. These values are in excellent agreement with those obtained from the Monte Carlo simulations, and they are shown as gray dots (turquoise online) in Fig. 1.

The results for Model B that are included in Fig. 1 were also obtained from Monte Carlo simulations of 2^{25} generations. (See Sec. 4 for further details.) The parameter values used in the figure were extracted as the average values from thirteen QSS communities identified in twelve independent simulation runs: $\overline{\mathcal{E}} = 0.61 \pm 0.04$ and $\overline{\Theta} = -0.15 \pm 0.01$. The value of the total population size given in the figure is the total time average over the simulations, averaged over all twelve runs, $\overline{N}_{\text{tot}} = 7726 \pm 303$. (Like for Model A, averages over only the particular observed QSS communities agree with this total average to within the error bars.) The large uncertainty in $\overline{N}_{\text{tot}}$ in this case is a direct consequence of the steep slope of the phase diagram for Model B for values of Θ closely below its critical value of zero.

3.4 Stability of fixed-point community

The internal stability of an \mathcal{N} -species fixed-point community is obtained from the matrix of partial derivatives,

$$\left. \frac{\partial n_I(t+1)}{\partial n_J(t)} \right|_{|n^*} = \delta_{IJ} + \Lambda_{IJ}, \quad (14)$$

where δ_{IJ} is the Kronecker delta function and Λ_{IJ} are elements of the *community matrix* $\mathbf{\Lambda}$ (Murray, 1989). Straightforward differentiation yields

$$\Lambda_{IJ} = \left(1 - \frac{1}{F} \right) \frac{n_I^*}{N_{\text{tot}}^*} \left[M_{IJ} - \frac{R\eta_I + (\hat{\mathbf{M}}|n^*)_I}{N_{\text{tot}}^*} - \frac{1}{N_0} \right], \quad (15)$$

where $(\hat{\mathbf{M}}|n^*)_I$ is the element of the column vector $\hat{\mathbf{M}}|n^*$, corresponding to species I . In order for deviations from the fixed point to decay monotonically,

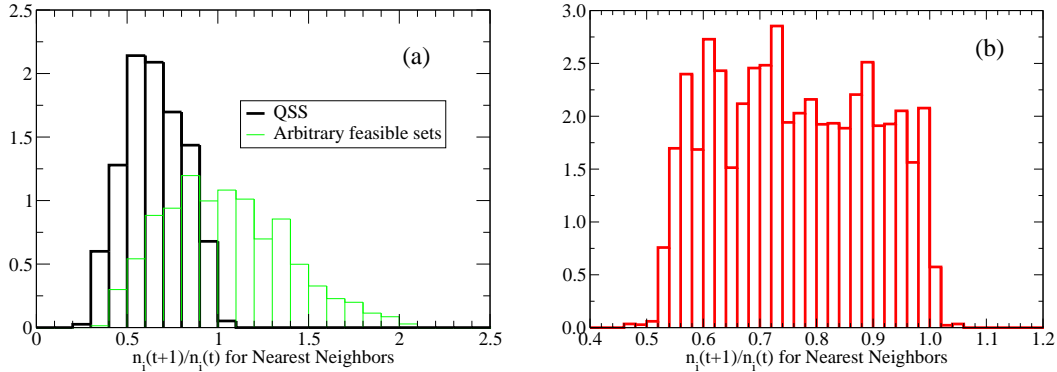


Fig. 4. (Color online.) Normalized histograms of the invader growth rates (exponential of the invasion fitness) for nearest-neighbor species of a QSS community for both models. **(a)** Histograms for Model A, based on the ten specific QSS included in Table I of Rikvold and Zia (2003) (thick, black lines), compared with the results for arbitrary, feasible, and internally stable communities [thin, gray lines (green online)]. After Rikvold and Zia (2003). **(b)** Histograms based on thirteen QSS communities identified from simulations of Model B.

cally in magnitude, the magnitudes of the eigenvalues of the matrix of partial derivatives in Eq. (14), $\mathbf{\Lambda} + \mathbf{1}$ where $\mathbf{1}$ is the \mathcal{N} -dimensional unit matrix, must be less than unity. The values of the fecundity F that are used in this work (4 for Model A and 2 for Model B) were chosen to satisfy this requirement for $\mathcal{N} = 1$.

Since new species are created by mutations, we must also study the stability of the fixed-point community toward “invaders.” Consider a mutant invader i . Then its multiplication rate, in the limit that $n_i \ll n_J$ for all \mathcal{N} species J in the resident community, is given by

$$\frac{n_i(t+1)}{n_i(t)} = \frac{F}{1 + \exp[-\Delta_i(R, \{n_J^*\})]}. \quad (16)$$

The Lyapunov exponent, $\ln[n_i(t+1)/n_i(t)]$, is the *invasion fitness* of the mutant with respect to the resident community (Metz et al., 1992; Doebeli and Dieckmann, 2000). A characteristic feature of the QSS communities observed in both Model A and Model B is that very few of the mutants that are separated from the resident community by a single mutation (“nearest-neighbor species”) have multiplication rates above unity. In fact, this is true only to a slightly lesser degree for mutants separated by two or three mutations from the resident species (“next-nearest neighbors” and “third-nearest neighbors”). Thus, a string of rather unsuccessful, or at best neutral, mutations is necessary to bring significant change to a QSS community – a fact that to a large extent accounts for their high degree of stability. This effect is illustrated for both models in Fig. 4.

4 Comparison of Dynamical Features

In this section we go beyond the mean-field treatment of the previous sections to compare some of the dynamical features observed in long kinetic Monte Carlo simulations of Model A and Model B. These simulations and their results were described in detail for Model A by Rikvold and Zia (2003), and further details for Model B will be reported elsewhere (Rikvold, in preparation). For both models we performed multiple simulations of $2^{25} = 33\,554\,432$ generations³ with a genome of length $L = 13$ ($2^{13} = 8192$ potential species) and a mutation rate per individual of $\mu = 10^{-3}$. The fecundity F was set to 4 for Model A and 2 for Model B.

The model parameters used in our simulations are chosen for computational feasibility with a view to keeping the system in the realistic regime where $\mathcal{N}(t) \ll 2^L$ and $\mathcal{N}(t) \ll N_{\text{tot}}(t)$ at all times. At the same time, we are interested in studying the dynamics during the stationary regime, which should therefore be reached in a reasonable time. As a result of these restrictions, L , R , and N_0 are quite small, while μ is quite large, compared to natural populations. Results of tests with larger L and R and smaller μ are summarized in Appendix B. These tests indicate that the product $R\mu$ is proportional to the average number of mutant individuals produced per generation, $\overline{N_{\text{tot}}}\mu$. We also note that this number is half of the *universal biodiversity number* in Hubbell’s neutral theory of biodiversity (Hubbell, 2001, Ch. 5). Even though the species in the models studied here are strongly interacting, this parameter appears to play a similar role as it does in the neutral theory. Furthermore, the power laws that are observed and discussed in this section are found to be robust, even against parameter changes that change $R\mu$.

In addition to the total population sizes shown in Fig. 3, we also studied the diversities of the resulting communities, defined as the number of major resident species. In order to obtain an approximation for the number of major species [which can be thought of as the wildtypes in a quasi-species model (Eigen, 1971; Eigen et al., 1988)], we filter out the low-population species that are most likely unsuccessful mutants of the wildtypes. This is achieved by using the exponential Shannon-Wiener diversity index (Krebs, 1989),

$$D(t) = e^{S[\{n_i(t)\}]} , \tag{17}$$

³ The simulation length was chosen as a power of two to enable use of the Fast Fourier Transform algorithm in calculating power spectral densities (Press et al., 1992, Chs. 12 and 13) (see below).

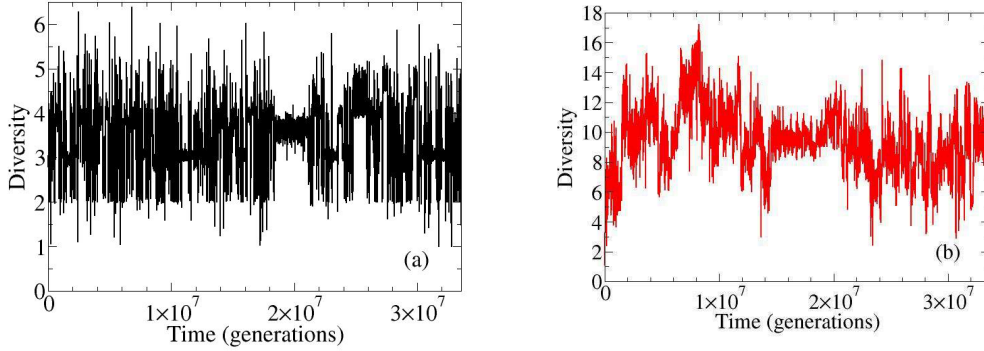


Fig. 5. (Color online.) Typical time series of the exponential Shannon-Wiener diversity index $D(t)$ in the same 2^{25} -generations Monte Carlo runs shown in Fig. 3. To reduce the size of the figure file, the data were downsampled as in Fig. 3. **(a)** Model A. **(b)** Model B.

where

$$S[\{n_I(t)\}] = - \sum_{\{I|\rho_I(t)>0\}} \rho_I(t) \ln \rho_I(t) \quad (18)$$

with $\rho_I(t) = n_I(t)/N_{\text{tot}}(t)$ is the information-theoretical entropy (Shannon, 1948; Shannon and Weaver, 1949). Typical time series for $D(t)$ in the two models are shown in Fig. 5. Just like in the time series for the total population sizes, the intermittent structure consisting of QSS on different timescales, separated by periods of high evolutionary activity, is clearly seen.

Statistical information for several characteristic times that describe the dynamics can be extracted from our data. One such time is the duration of a QSS. One way to determine this is to use a cutoff on the size of the diversity fluctuations, whose probability densities for the two models are shown in Fig. 6(a). In both cases, the probability densities consist of a Gaussian central part representing the fluctuations during the QSS periods (Zia and Rikvold, 2004), flanked by “wings” that correspond to the large fluctuations during the evolutionarily active periods. We choose a cutoff $y_c = 0.015$ for Model A and 0.010 for Model B, in both cases corresponding to the transition region between the Gaussian central peak and the wings. The duration of a single QSS then corresponds to the time interval between consecutive times when $|dS(t)/dt|$ exceeds y_c . Log-log plots of the resulting probability densities for the durations of QSS in the two models are shown together in Fig. 6(b). While both show approximate power-law behavior over five decades or more in time, there is an important difference: the power-law exponent for Model A is near -2 , while for Model B it is closer to -1 .

A different time of interest is the lifetime of a particular species, defined as the time elapsed between its origination and eventual extinction. Log-log plots of

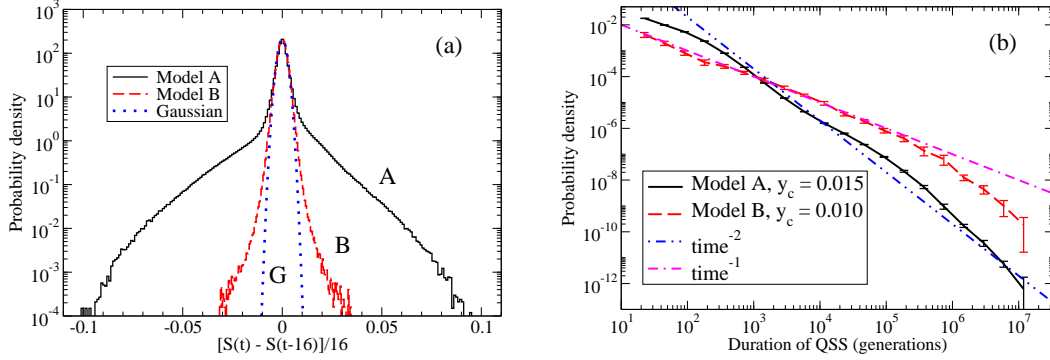


Fig. 6. (Color online.) **(a)** Normalized histograms representing the probability density of the logarithmic derivative of the diversity, $dS(t)/dt$. The data were averaged over 16 generations in each run, and then averaged over 16 independent runs for Model A (solid, marked A) and 12 runs for Model B (dashed, marked B). The central parts of both histograms are well fitted by a Gaussian (dotted, marked G). **(b)** Log-log plot of normalized histograms representing the probability density of the durations of QSS, estimated as the periods between times when $|dS(t)/dt|$ exceeds a cutoff y_c ($dS(t)/dt$ was averaged over 16 generations as in part (a)). Model A (solid) and Model B (dashed). Results for Model A were averaged over 16 runs, and for Model B over 12 runs. The error bars are standard errors, based on the spread between runs. The two dot-dashed straight lines represent time^{-2} and time^{-1} power laws, respectively.

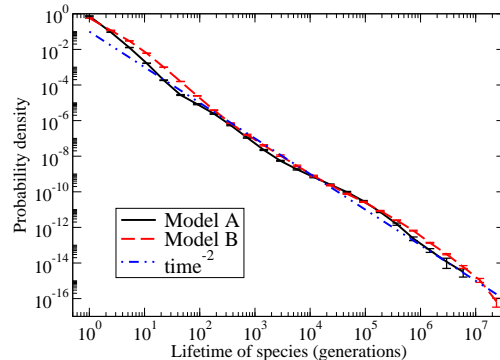


Fig. 7. (Color online.) Log-log plot of normalized histograms representing the probability density of the lifetime of a particular species. Model A (solid) and Model B (dashed). Results for Model A were averaged over eight runs, and for Model B over 12 runs. The error bars were calculated as in Fig. 6(b). The dot-dashed straight line represents a time^{-2} power law.

histograms of the species lifetimes in the two models are shown in Fig. 7. In contrast to the case of the QSS durations, the species-lifetime distributions are very close for the two models, both showing approximate time^{-2} behavior over near seven decades in time. The observed exponent is significantly different from $-3/2$, which would correspond to the simple hypothesis that the lifetime distributions simply correspond to the first-return-time distribution for a random walk of n_I (Newman and Palmer, 2003, Ch. 1). Lifetime distributions for marine genera that are compatible with a power law with an

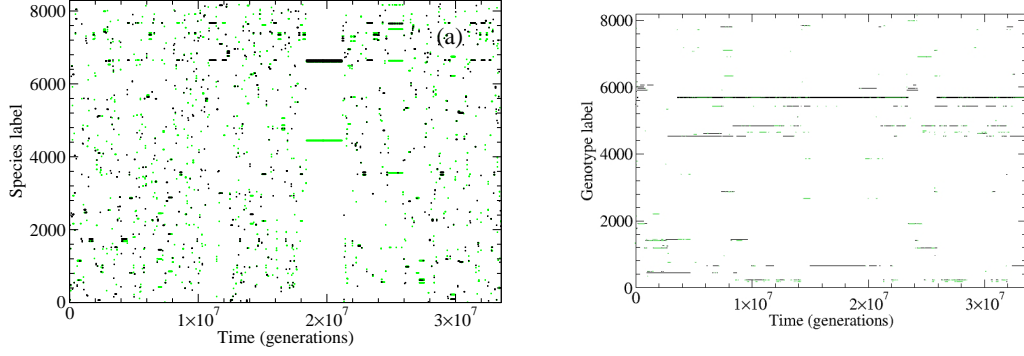


Fig. 8. (Color online.) Plots showing the labels I of the most highly populated species vs time. The data are for the same 2^{25} -generation Monte Carlo runs shown in Figs. 3 and 5. Gray (green online): $n_I \in [101, 1000]$. Black: $n_I \geq 1001$. **(a)** Model A. **(b)** Model B. For clarity, only producer species are shown for this model. The consumer species give a similar picture. See further discussion in the text.

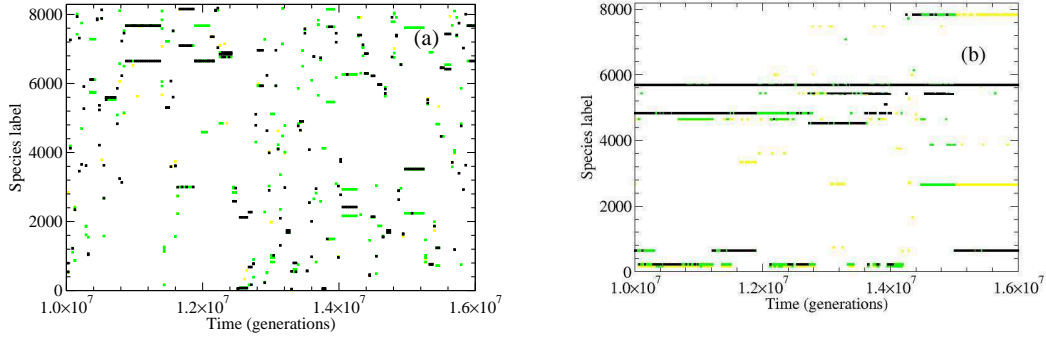


Fig. 9. (Color online.) Magnified version of Fig. 8, showing times between 1.0×10^7 and 1.6×10^7 generations. In addition to the species shown in Fig. 8, the ones with $n_I \in [11, 100]$ are also shown (light gray, yellow online). **(a)** Model A. **(b)** Model B. See further discussion in the text.

exponent in the range -1.5 to -2 have been obtained from the fossil record (Newman and Sibani, 1999; Newman and Palmer, 2003, Ch. 1). However, the possible power-law behavior in the fossil record is only observed over about one decade in time – between 10 and 100 million years – and other fitting functions, such as exponential decay, are also possible. Nevertheless, it is reasonable to conclude that the numerical results obtained from complex, interacting evolution models that extend over a large range of time scales support interpretations of the fossil lifetime evidence in terms of nontrivial power laws.

The difference in the power laws for the QSS durations and the species lifetimes is a puzzling result. One possible explanation can be gleaned from the data shown in Figs. 8 and 9. These show the species labels of highly populated species as functions of time for both models. From Figs. 8(a) and 9(a) it is seen that all or most of the horizontal lines representing populated species at a

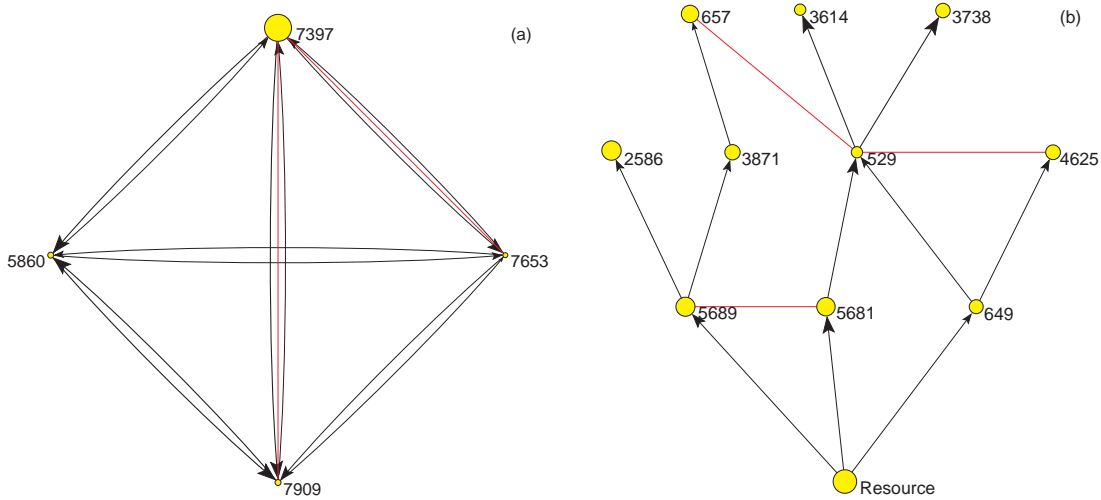


Fig. 10. (Color online.) Typical QSS communities observed in simulations of the two models. The numbers are the species labels I , and the sizes of the circles represent the individual species' steady-state populations. A black arrow pointing toward species I indicates a positive M_{IJ} , with magnitude indicated by the line thickness and size of the arrow head. The thin gray lines (red online) connect nearest neighbors in genotype space. (a) Model A. This particular QSS community is the one included in Table 2 of Zia and Rikvold (2004) and line 10 of Table I of Rikvold and Zia (2003). (b) Model B. This is the food web representing the QSS community existing between 15 and 18 million generations in the simulation shown in Figs. 3(b), 5(b), 8(b), and 9(b). It has three trophic levels above the resource node.

given time for Model A start and stop almost simultaneously, indicating that species originations and extinctions in this model are highly synchronized. In other words: whole communities in Model A tend to go extinct and be replaced with an entirely new community within a short time. In contrast, in Figs. 8(b) and 9(b) the different horizontal species lines for Model B stop and start at different times. This indicates that communities in this model are much more robust, and extinction events seldom wipe out more than a part of the total community. Thus, QSS would be expected to be more long-lived (but also less clearly defined) for Model B, than for Model A. This theory is supported by the strikingly different QSS community structures produced by the two models, shown in Fig. 10. The typical QSS community shown for Model A is a small cluster of mutualistically interacting species, while the typical community shown for Model B has the character of a simple food web. Extinctions in the latter are likely to be confined to a single branch of the web.

The arbitrariness inherent in the cutoff that must be used to extract QSS duration distributions from fluctuations in the diversity or other time series can to some extent be eliminated by mapping distributions obtained with different cutoffs onto a common scaling function (Paczuski et al., 1996; Rikvold,

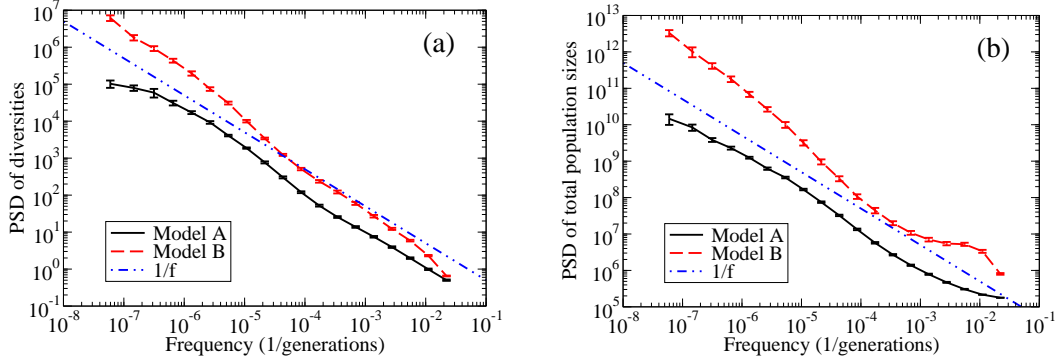


Fig. 11. (Color online.) Log-log plots of PSDs of (a) the diversities $D(t)$ and (b) the total population sizes $N_{\text{tot}}(t)$ for Model A and Model B. The PSDs are averaged over each octave in frequency, and then over 16 runs for Model A and 12 runs for Model B. The error bars were calculated as in Fig. 6(b). The dashed straight lines represent $1/f$ power-law behavior.

2005). However, an analysis method that completely avoids any cutoffs is that of calculating power spectral densities (the square of the temporal Fourier transform). Power spectra (PSDs) are therefore shown in Fig. 11 for both models. The PSDs for the diversity are shown in Fig. 11(a), and for the total population size in Fig. 11(b). Although there are clear deviations, the overall behaviors for both quantities and for both models are compatible with a $1/f$ power law over many decades in frequency. In the high-frequency regime the population-size PSDs have a significant background of noise, presumably caused by the rapid population fluctuations due to the birth and death of individual organisms. For very low frequencies there is little reason to believe that there should be large differences between the behaviors of the two quantities for the same model. We therefore think it is reasonable to consider the difference between the slopes of the diversity and population-size PSDs for Model A as an indication of the true uncertainty in the PSDs at the lowest frequencies. Better estimates in this regime would require several orders of magnitude longer simulations.

5 Discussion and Conclusions

In this paper we have introduced a class of individual-based models of biological coevolution, and we have shown that a simplified subclass of these models is amenable to analytic linear stability calculations. Since the simplification involves universal competition and ignores important effects such as adaptive foraging, the resulting models are not highly realistic. However, the fact that the results of numerical simulations can be compared with analytical results make these simplified models ideal as benchmarks for simulations of more realistic models in the future.

A central result of the analytic study is that, in the absence of mutations, the total population size of a fixed-point community, N_{tot}^* , is described by a model with a community fitness function that is cubic in N_{tot}^* . In addition to the present application, such a model is also applicable to nonequilibrium phase transitions in such diverse systems as epidemics, lasers, and autocatalytic chemical reactions. However, the evolution models studied here differ from those kinds of systems by the important effect that, in the *presence* of mutations, the model parameters Θ and \mathcal{E} are no longer externally imposed constraints, but rather *evolve* as far in the direction of positive Θ as allowed by the internal constraints of the particular model. As a result, Model A, in which the elements of the interspecies interaction matrix \mathbf{M} are randomly distributed on an interval that is symmetric about zero, evolves to produce communities that are heavily biased toward mutualism. The effective interaction variable Θ adjusts to a positive value, where a community of nonzero population size can exist *without* an external resource. In contrast, the predator/prey Model B, in which the interspecies interactions are antisymmetric, is constrained to nonpositive values of Θ , for which a nonzero population size can only be sustained through an external resource. These results are illustrated in Fig. 1(a).

In a recent study of a similar, but different model for coevolution, Tokita and Yasutomi (2003) also observed the emergence of strongly mutualistic communities from initially unbiased conditions. In their model, mutants are very similar to their parents, except for their interactions with a few other species (“local mutations” in the words of those authors), and they suggest that the evolution of mutualism is related to this feature of their model. However, the mutations in our models would be “global” in the language of Tokita and Yasutomi, which leads us to the conclusion that the emergence of mutualism is common in models where direct mutualistic interactions are allowed. Rather remarkably, we have found little difference in the dynamics between the version of Model A studied in this paper and a version with strongly correlated interactions, and thus more “local” mutations (Sevim and Rikvold, 2005). It remains an important problem to reconcile this tendency for evolution of mutualism with the obvious requirement that biomass cannot be created without energy input. While predator/prey interactions are easy to reconcile with energy conservation, direct mutualistic interactions (although effective mutualism is common in nature (Kawanabe et al., 1993; Bronstein, 1994; Krebs, 2001, Ch. 14)) are more difficult to interpret in an energy framework (Bronstein, 1994). We believe this emphasizes the importance of distinguishing between *direct* mutualistic interactions, as in Model A, and *effective* mutualisms, which merely mean that a pair of elements in the community matrix, Λ_{IJ} and Λ_{JI} , are both positive.

Beyond the mean-field studies and the simulation results for average population sizes, we have also studied the temporal fluctuations of both the diversity

and total population size for Models A and B. We find that the probability distributions of the lifetimes of individual species in both models are very similar, showing power-law decay with an exponent near -2 over near seven decades in time, as seen in Fig. 7. This exponent value is consistent with some interpretations of the available data for the lifetimes of marine genera in the fossil record (Newman and Sibani, 1999; Newman and Palmer, 2003, Ch. 1), but other interpretations of the fossil evidence are also possible. Similarly, power spectra for the diversity, as well as for the total population size, show reasonable (although not perfect) $1/f$ behavior over many decades in frequency, as seen in Fig. 11. It is therefore very interesting that the probability distributions of the durations of individual QSS periods in the two models also both show reasonable power-law decay, but with *different* exponents: near -2 for Model A and close to -1 for Model B, as seen in Fig. 6(b). This result, which we found quite surprising at first, makes sense in light of the observation that the extinctions of major species are highly synchronized in Model A, while they are much less so in Model B. While communities in Model A tend to collapse completely when an aggressive mutant arrives and/or a major species goes extinct, communities in Model B are much more resilient and extinctions most often only extend to one or a few branches of the resident food web. This effect is illustrated in Figs. 8, 9, and 10.

Our observation of the high resilience of Model B against complete extinction of communities is consistent with observations of extinction avalanches of limited size in the Web-world model by Drossel et al. (2001), who argue that their model is therefore *not* self-organized critical. Together with our observation of the self-optimization of the class of evolution models studied here to points *away from* the transcritical bifurcation point, these observations may support a conclusion that models of coevolution that take reasonable account of the dynamics at the ecological level (even if they are extremely simplified) are not in general self-organized critical. Such a conclusion would be in disagreement with a number of recent theories of extinction (Bak and Sneppen, 1993; Newman and Palmer, 2003, and references therein).

The results presented here indicate that further work on models of macroevolution that are based on events on ecological time scales, with comparisons of the results with data from the fossil record, as well as from laboratory experiments and extant food webs, is highly desirable. In a forthcoming paper we will consider in detail the structure and dynamics of the food webs that develop within Model B (Rikvold, in preparation).

Acknowledgments

The author thanks R. K. P. Zia, B. Schmittmann, P. Beerli, G. J. P. Naylor, and V. Sevim for useful discussions and comments on the manuscript, and V. Sevim for the data on Model A included in Fig. 7. He also gratefully acknowledges hospitality at Kyoto University by H. Tomita in the Department of Fundamental Sciences, Faculty of Integrated Human Studies, and H. Fujisaka in the Department of Applied Analysis and Complex Dynamical Systems, Graduate School of Informatics.

This work was supported in part by U.S. National Science Foundation Grants No. DMR-0240078 and DMR-0444051, and by Florida State University through the School of Computational Science, the Center for Materials Research and Technology, the National High Magnetic Field Laboratory, and a COFRS summer-salary grant.

A Derivation of the Community Fitness Function

In this Appendix we provide a conventional derivation of the cubic form of the community fitness function $\Phi(N_{\text{tot}})$ in a simple mean-field approximation. The derivation provides an explanation for the prefactor $(1 - 1/F)$ in Eq. (11), as well as intuitively clear approximations for the coefficients Θ and \mathcal{E} . It also provides justification that the equation to be integrated to obtain $\Phi(N_{\text{tot}})$ is indeed Eq. (7), rather than this equation multiplied or divided by some power of N_{tot} . The derivation is based on the time-dependent Ginzburg-Landau equation for a system with nonconserved order parameter (Hohenberg and Halperin, 1977; Goldenfeld, 1992, Ch. 8.3), which for our current systems takes the form

$$\frac{\partial N_{\text{tot}}}{\partial t} = \frac{\partial \Phi}{\partial N_{\text{tot}}}. \quad (\text{A.1})$$

(The fitness Φ is the negative of the Landau free energy customarily considered in physics applications.)

Identifying $\partial n_I(t)/\partial t$ with $n_I(t+1) - n_I(t)$, we obtain from Eqs. (1–3) in the absence of mutations:

$$\frac{\partial n_I(t)}{\partial t} = n_I(t) \left\{ \frac{F}{1 + \exp \left[b_I - \frac{\eta_I R}{N_{\text{tot}}(t)} - \sum_J M_{IJ} \frac{n_J(t)}{N_{\text{tot}}(t)} + \frac{N_{\text{tot}}(t)}{N_0} \right]} - 1 \right\}. \quad (\text{A.2})$$

Expanding this nonlinear equation of motion around its fixed point, we get

$$\frac{\partial n_I(t)}{\partial t} \approx \left(1 - \frac{1}{F}\right) n_I(t) \left[-\tilde{b}_I + \frac{\eta_I R}{N_{\text{tot}}(t)} + \sum_J M_{IJ} \frac{n_J(t)}{N_{\text{tot}}(t)} - \frac{N_{\text{tot}}(t)}{N_0} \right]. \quad (\text{A.3})$$

To obtain the simplest mean-field approximation for $\partial N_{\text{tot}}/\partial t$ (exact for $\mathcal{N} = 1$), we set $n_I \approx N_{\text{tot}}/\mathcal{N}$, $\tilde{b}_I \approx \mathcal{N}^{-1} \sum'_I \tilde{b}_I \equiv \langle \tilde{b} \rangle$, $\eta_I \approx \mathcal{N}^{-1} \sum'_I \eta_I \equiv \langle \eta \rangle$, and $M_{IJ} \approx \mathcal{N}^{-2} \sum'_{IJ} M_{IJ} \equiv \langle M \rangle$, where the primes on the sums indicate that they are restricted to the \mathcal{N} species with $n_I > 0$. This yields

$$\frac{\partial N_{\text{tot}}}{\partial t} \approx \left(1 - \frac{1}{F}\right) \left[R \langle \eta \rangle + (\langle M \rangle - \langle \tilde{b} \rangle) N_{\text{tot}} - \frac{(N_{\text{tot}})^2}{N_0} \right]. \quad (\text{A.4})$$

Integrating the right-hand side as prescribed by Eq. (A.1), we find

$$\Phi(N_{\text{tot}}) \approx \left(1 - \frac{1}{F}\right) \left(R \langle \eta \rangle N_{\text{tot}} + \frac{\langle M \rangle - \langle \tilde{b} \rangle}{2} N_{\text{tot}}^2 - \frac{1}{3N_0} N_{\text{tot}}^3 \right). \quad (\text{A.5})$$

This result has the same cubic form as Eq. (11), with the approximate coefficients $\langle \eta \rangle \approx \mathcal{E}$ and $(\langle M \rangle - \langle \tilde{b} \rangle) \approx \Theta$. The exact fixed-point solution for N_{tot} requires the use of \mathcal{E} and Θ , but the approximate forms obtained here provide a more intuitive understanding of the significance of these coefficients.

B Trials with Other Parameter Values

In addition to the parameter set used in the main simulations presented above, we also performed trial simulations for Model B with $L = 20$ (1 048 576 potential species), $\mu = 2.5 \times 10^{-4}$, and $R = 8000$. As each simulation run with $R = 2000$ took about two weeks of CPU time, and each run with $R = 8000$ took at least four weeks, relatively few trial runs were performed. No qualitative differences were observed in the quantities reported on the basis of the main simulation series.

To obtain estimates of the effects of L , μ , and R on the the mean stationary levels of the total population size, $\overline{N_{\text{tot}}}$, and diversity, \overline{D} , and the mean time to reach stationarity, $\overline{\tau}$, we fitted these variables by the exponential function $a[1 - \exp(-t/\tau)]$. Numerical results for $\overline{\tau}$, \overline{D} , and $\overline{N_{\text{tot}}}$, based on twelve runs for $L = 13$, $R = 2000$, and $\mu = 10^{-3}$ (the original runs used in the main part of this paper); twelve runs for $L = 20$, $R = 2000$, and $\mu = 10^{-3}$; nine runs for $L = 20$, $R = 2000$, and $\mu = 2.5 \times 10^{-4}$; and five runs for $L = 20$, $R = 8000$, and $\mu = 2.5 \times 10^{-4}$ are compiled in Table B.1.

Table B.1

Numerical results for the main simulations of Model B with $L = 13$, compared with trial runs with $L = 20$ and varying R and μ . The unit for R and $\overline{N}_{\text{tot}}$ is individuals, for μ it is mutations per individual offspring per generation, for $\overline{\tau}$ it is 10^6 generations, and for \overline{D} it is species. Thus, $R\mu$ is proportional to the total number of mutated offspring per generation. The uncertainties are standard errors, based on the spread between individual runs. σ_τ is the standard deviation of τ over the independent runs. A ratio $\overline{\tau}/\sigma_\tau \approx 1$ indicates that τ may be approximately exponentially distributed, while the even lower ratio for $R\mu = 0.5$ indicates very large variations from run to run.

L	R	μ	$R\mu$	Runs	$\overline{\tau}$	$\overline{\tau}/\sigma_\tau$	\overline{D}	$\overline{N}_{\text{tot}}$
13	2000	10^{-3}	2.0	12	0.35 ± 0.07	1.08	10.9 ± 0.3	$7\,700 \pm 300$
20	2000	10^{-3}	2.0	12	0.8 ± 0.2	0.93	14.7 ± 0.3	$13\,700 \pm 400$
20	8000	2.5×10^{-4}	2.0	5	1.2 ± 0.3	0.90	20.4 ± 0.6	$58\,000 \pm 7\,000$
20	2000	2.5×10^{-4}	0.5	9	5 ± 2	0.53	10.3 ± 0.2	$12\,000 \pm 2\,000$

B.1 Large genome

With $L = 13$, the whole pool of potential species is visited in a typical 2^{25} -generation simulation, while only about 10% are typically visited for $L = 20$ with $\mu = 10^{-3}$ and $R = 2000$. However, the frequent ‘‘revival’’ of extinct species seen with $L = 13$ has no effect on the observed power laws. Twelve full runs were performed for this parameter set. All the subsequent trial simulations were performed with $L = 20$.

As expected from Eq. (12), \overline{D} appears to be proportional to L . The significant increase in $\overline{N}_{\text{tot}}$ when L is increased from 13 to 20 (not seen in trial runs with $L = 20$ for Model A) is probably due to the increased probability of finding species with smaller b and thus closer to the population divergence for Model B at $\Theta = 0$ (see Fig. 1(a)).

B.2 Effects of reduced μ and increased R

We found $\overline{\tau}$ to be approximately inversely proportional to μ and R , while the mean diversity increases (but apparently sublinearly) with both μ and R . Within the uncertainty, $\overline{\tau}$ was also the same for the diversity and population size, and the reported results are therefore based on both quantities. The mean total population size $\overline{N}_{\text{tot}}$ appears to be roughly independent of μ and approximately linearly dependent on R . This latter proportionality means that $R\mu \propto \overline{N}_{\text{tot}}\mu$, the average total number of mutant individuals per generation. Even though the models studied here have strong interspecies interactions, we

note that $\overline{N_{\text{tot}}}\mu$ is one half of the *fundamental biodiversity number* in Hubbell's neutral theory of biodiversity (Hubbell, 2001, Ch. 5). This parameter appears to play an analogous role in the present models as it does in the neutral theory.

However, more important than the above results is that none of the observed power laws changed under parameter variation within this range. In particular, the exponent for the PDF of individual species lifetimes remained near -2 for all parameter sets, while the exponent for the QSS duration PDF remained close to -1 . In fact, allowing for the larger overall intensity in the population PSD for $R = 8000$ and to within the numerical accuracy, both PDFs and PSDs for all three parameter sets with $L = 20$ can be overlaid graphically with the ones presented for $L = 13$, $\mu = 10^{-3}$, and $R = 2000$ elsewhere in this paper. Based on these trials we therefore conclude that the parameters used in the main study are also representative for systems with larger L and R and smaller μ and are well chosen to study the stationary dynamics of the models on long time scales.

References

- Armstrong, R. A., McGehee, R., 1980. Competitive exclusion. *Am. Naturalist* 115, 151–170.
- Bak, P., Sneppen, K., 1993. Punctuated equilibrium and criticality in a simple model of evolution. *Phys. Rev. Lett.* 71, 4083–4086.
- Bronstein, J. L., 1994. Our current understanding of mutualism. *Quart. Rev. Biol.* 69, 31–51.
- Caldarelli, G., Higgs, P. G., McKane, A. J., 1998. Modelling coevolution in multispecies communities. *J. theor. Biol.* 193, 345–358.
- Chowdhury, D., Stauffer, D., 2005. Evolutionary ecology in-silico: Does mathematical modelling help in understanding the generic trends? *J. Biosciences* 30, 277–287.
- Chowdhury, D., Stauffer, D., Kunwar, A., 2003. Unification of small and large time scales for biological evolution: Deviations from power law. *Phys. Rev. Lett.* 90, 068101.
- Christensen, K., di Collobiano, S. A., Hall, M., Jensen, H. J., 2002. Tangled-nature: A model of evolutionary ecology. *J. theor. Biol.* 216, 73–84.
- Crawford, J. D., 1991. Introduction to bifurcation theory. *Rev. Mod. Phys.* 63, 991–1037.
- Crosby, J. L., 1970. The evolution of genetic discontinuity: Computer models of the selection of barriers to interbreeding between subspecies. *Heredity* 25, 253–297.
- den Boer, P. J., 1986. The present status of the competitive exclusion principle. *Trends Ecol. Evol.* 1, 25–28.

- di Collobiano, S. A., Christensen, K., Jensen, H. J., 2003. The tangled nature model as an evolving quasi-species model. *J. Phys. A* 36, 883–891.
- Doebeli, M., Dieckmann, U., 2000. Evolutionary branching and sympatric speciation caused by different types of ecological interactions. *Am. Naturalist* 156, S77–S101, and references therein.
- Drossel, B., Higgs, P. G., McKane, A. J., 2001. The influence of predator-prey population dynamics on the long-term evolution of food web structure. *J. theor. Biol.* 208, 91–107.
- Drossel, B., McKane, A., Quince, C., 2004. The impact of non-linear functional responses on the long-term evolution of food web structure. *J. theor. Biol.* 229, 539–548.
- Dunne, J., Williams, R. J., Martinez, N. D., 2002. Network structure and diversity loss in food webs: Robustness increases with connectance. *Ecol. Lett.* 5, 558–567.
- Eigen, M., 1971. Selforganization of matter and evolution of biological macromolecules. *Naturwissenschaften* 58, 465.
- Eigen, M., McCaskill, J., Schuster, P., 1988. Molecular quasi-species. *J. Phys. Chem.* 92, 6881–6891.
- Garlaschelli, D., 2004. Universality in food webs. *Eur. Phys. J. B* 38, 277–285.
- Gavrilets, S., 1999. Dynamics of clade diversification on the morphological hypercube. *Proc. R. Soc. Lond. B* 266, 817–824.
- Gavrilets, S., 2004. *Fitness landscapes and the origin of species*. Princeton University Press, Princeton and Oxford.
- Gavrilets, S., Boake, C. R. B., 1998. On the evolution of premating isolation after a founder event. *Am. Naturalist* 152, 706–716.
- Gavrilets, S., Li, H., Vose, M. D., 2000. Patterns of parapatric speciation. *Evolution* 54, 1126–1134.
- Gavrilets, S., Vose, A., 2005. Dynamic patterns of adaptive radiation. *Proc. Natl. Acad. Sci. USA* 102, 18040–18045.
- Goldenfeld, N., 1992. *Lectures on Phase Transitions and the Renormalization Group*. Addison-Wesley, Reading, MA.
- Haken, H., 1977. *Synergetics – An Introduction*. Springer-Verlag, Berlin.
- Hall, M., Christensen, K., di Collobiano, S. A., Jensen, H. J., 2002. Time-dependent extinction rate and species abundance in a tangled-nature model of biological evolution. *Phys. Rev. E* 66, 011904.
- Hardin, G., 1960. The competitive exclusion principle. *Science* 131, 1292–1297.
- Hohenberg, P. C., Halperin, B., 1977. Theory of dynamic critical phenomena. *Rev. Mod. Phys.* 49, 435–479.
- Hubbell, S. P., 2001. *The Unified Neutral Theory of Biodiversity and Biogeography*. Princeton University Press, Princeton.
- Kauffman, S. A., 1993. *The origins of order. Self-organization and selection in evolution*. Oxford University Press, Oxford.
- Kauffman, S. A., Johnsen, S., 1991. Coevolution to the edge of chaos: Coupled fitness landscapes, poised states, and coevolutionary avalanches. *J. theor. Biol.* 149, 467–505.

- Kawanabe, H., Cohen, J. E., Iwasaki, K., 1993. *Mutualism and Community Organization*. Oxford University Press, Oxford.
- Krebs, C. J., 1989. *Ecological Methodology*. Harper & Row, New York, chap. 10.
- Krebs, C. J., 2001. *Ecology. The Experimental Analysis of Distribution and Abundance*. Fifth Edition. Benjamin Cummings, San Francisco.
- Metz, J. A. J., Nisbet, R. M., Geritz, S. A. H., 1992. How should we define ‘fitness’ for general ecological scenarios? *Trends Ecol. Evol.* 7, 198–202.
- Murray, J. D., 1989. *Mathematical Biology*. Springer-Verlag, Berlin.
- Newman, M. E. J., Palmer, R. G., 2003. *Modeling Extinction*. Oxford University Press, Oxford.
- Newman, M. E. J., Sibani, P., 1999. Extinction, diversity and survivorship of taxa in the fossil record. *Proc. R. Soc. Lond. B* 266, 1583–1599.
- Paczuski, M., Maslov, S., Bak, P., 1996. Avalanche dynamics in evolution, growth, and depinning models. *Phys. Rev. E* 53, 414–443.
- Pathria, R. K., 1996. *Statistical Mechanics, Second Edition*. Butterworth-Heinemann, Oxford.
- Press, W. H., Teukolsky, S. A., Vetterling, W. T., Flannery, B. P., 1992. *Numerical Recipes, Second Ed.* Cambridge University Press, Cambridge.
- Rikvold, P. A., 2005. Fluctuations in models of biological macroevolution. In: Kish, L. B., Lindenberg, K., Gingl, Z. (Eds.), *Noise in Complex Systems and Stochastic Dynamics III*. SPIE, The International Society for Optical Engineering, Bellingham, WA, pp. 148–155, e-print arXiv:q-bio.PE/0502046.
- Rikvold, P. A., in preparation. Fluctuations and food webs in an individual-based predator/prey model of biological coevolution.
- Rikvold, P. A., Zia, R. K. P., 2003. Punctuated equilibria and $1/f$ noise in a biological coevolution model with individual-based dynamics. *Phys. Rev. E* 68, 031913.
- Roberts, A., 1974. The stability of a feasible random ecosystem. *Nature (London)* 251, 607–608.
- Sevim, V., Rikvold, P. A., 2005. Effects of correlated interactions in a biological coevolution model with individual-based dynamics. *J. Phys. A* 38, 9475–9489.
- Shannon, C. E., 1948. A mathematical theory of communication. *Bell Syst. Tech. J.* 27, 379–423; 628–656.
- Shannon, C. E., Weaver, W., 1949. *The Mathematical Theory of Communication*. University of Illinois Press, Urbana.
- Solé, R. V., Bascompte, J., Manrubia, S., 1996. Extinction: Bad genes or weak chaos? *Proc. R. Soc. Lond. B* 263, 1407–1413.
- Strogatz, S. H., 1994. *Nonlinear Dynamics and Chaos*. Westview Press, Boston.
- Thompson, J. N., 1998. Rapid evolution as an ecological process. *Trends Ecol. Evol.* 13, 329–332.
- Thompson, J. N., 1999. The evolution of species interactions. *Science* 284, 2116–2118.

- Tokita, K., Yasutomi, A., 2003. Emergence of a complex and stable network in a model ecosystem with extinction and mutation. *Theor. Popul. Biol.* 63, 131–146.
- Verhulst, P. F., 1838. Notice sur la loi que la population suit dans son accroissement. *Corres. Math. et Physique* 10, 113–121.
- Yoshida, T., Jones, L. E., Ellner, S. P., Fussmann, G. F., Hairston, N. G., 2003. Rapid evolution drives ecological dynamics in a predator-prey system. *Nature* 424, 303–306.
- Zia, R. K. P., Rikvold, P. A., 2004. Fluctuations and correlations in an individual-based model of biological coevolution. *J. Phys. A* 37, 5135–5155.